Baghdad Science Journal

Volume 23 | Issue 6 Article 3

6-17-2026

Novel Engineering of Nickel Oxide and Chromium Oxide Nanocomposites for Anti-Corrosion Studies

Sahar Ismael Imran
Department of Basic Science, College of Dentistry, Mustansiriyah University, Baghdad, Iraq,
sa7ar9x9@uomustansiriyah.edu.iq

How to Cite this Article

Imran, Sahar Ismael (2026) "Novel Engineering of Nickel Oxide and Chromium Oxide Nanocomposites for Anti-Corrosion Studies," *Baghdad Science Journal*: Vol. 23: Iss. 6, Article 3.
DOI: https://doi.org/10.21123/2411-7986.5318

BAGHDAD SCIENCE JOURNAL 2026;23(6):2012–2024

RESEARCH ARTICLE

Novel Engineering of Nickel Oxide and Chromium Oxide Nanocomposites for Anti-Corrosion Studies

Sahar Ismael Imran

Department of Basic Science, College of Dentistry, Mustansiriyah University, Baghdad, Iraq

ABSTRACT

Mixed nickel oxide/chromium oxide nanocomposites NCs (NiO/Cr_2O_3 NCs) have been synthesized via two distinct routes, the first: a green direct calcination-microwave-assisted route (sample B1) of nickel and chromium salts in a crucible within an enclosed oven chamber, which provides an environmentally friendly approach free of gaseous and fluid waste. The second is a conventional co-precipitation-microwave-assisted technique (sample B2). Both methods produced a novel bio-inspired hierarchical micro-lobed architecture pattern. The corrosion resistance effects of both samples have been studied. NiO/Cr_2O_3 NCs were characterized using a field emission scanning electron microscope, X-ray diffractometer, EDX-ray spectroscope, and FT-IR Fourier transform infrared. XRD analysis confirmed average crystallite sizes of 22.93 nm (B1) and 23.24 nm (B2), whereas AFM measurements indicated mean particle sizes of 40–45 nm, suggesting well-defined nanocrystals with minimal agglomeration. Despite significant differences in Ni/Cr composition (B1:~1.3 vs. B2:~2.3) from EDS, both (NiO/Cr_2O_3 NCs) were found to have comparable corrosion inhibition efficiencies of ~82% when carbon steel was added to (0.1) M of HCl. The assessments of electrochemical analysis identified the primary mechanism as the formation of a protective/shielding layer on the steel surface. These findings indicate that anti-corrosion performance is largely governed by barrier formation rather than stoichiometry, validating both synthesis routes as sustainable strategies for designing high-performance NiO/Cr_2O_3 NCs as anti-corrosion materials, effectively preventing corrosion.

Keywords: Co-precipitation method, Corrosion resistance, Direct calcination method, Metal oxide nanoparticles, Morphological properties, Structural properties

Introduction

Carbon steel corrosion in an acidic environment represents a persistent and costly challenge for numerous industrial sectors; thus, the pursuit of effective, advanced, and environmentally compliant corrosion inhibitors is a critical research endeavor.[1,2] Metal oxide nanocomposites (MONCs) have become an encouraging addition to this field[3] with chromium oxide (Cr_2O_3) and nickel oxide (NiO) being particularly promising due to their high-temperature resistance, stability, and electrochemical properties.[4,5] The combination of these metal oxides in nanocomposite structures has shown superior performance across various applications, though their full potential as a protective barrier and corrosion inhibition remains underexplored.[6]

While the singular properties of NiO and Cr_2O_3 nanoparticles are well established, studies on their nanocomposites for corrosion protection are underdeveloped, with the few reported studies focusing on their electrical conductivity,[7] energy storage devices like supercapacitors,[8] and more recently exploring photocatalytic properties.[9] This leaves a huge research gap in the systematic study of synthesis methods for NiO/Cr_2O_3 NCs and a basic understanding of how such synthesis methods influence their anti-corrosion mechanism. In order to achieve this, the present work introduces a new, green direct calcination method (B1) and compares it

Received 14 April 2025; revised 4 January 2026; accepted 6 January 2026.
Available online 17 June 2026

E-mail address: sa7ar9x9@uomustansiriyah.edu.iq (S. I. Imran).

https://doi.org/10.21123/2411-7986.5318

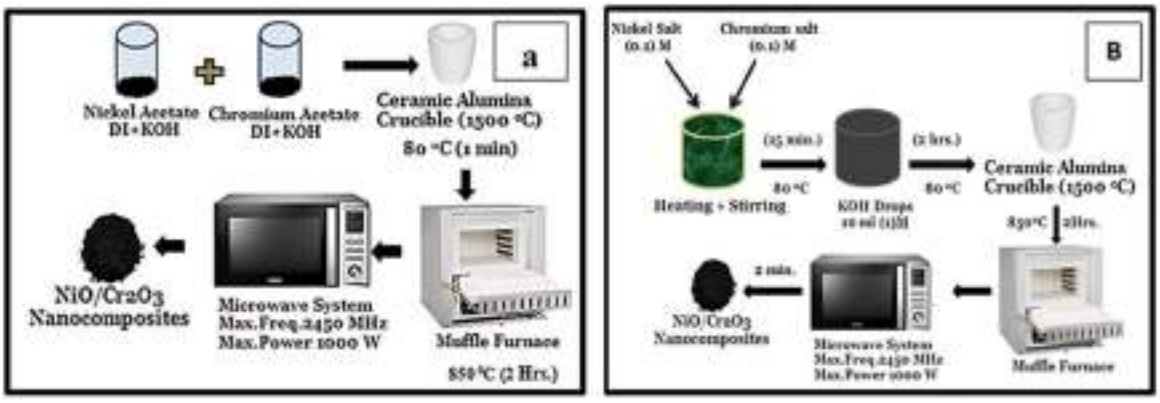

Scheme 1. (a) Synthesis of of NiO/Cr_2O_3NCs via direct thermal decomposition method. (b) Synthesis of of NiO/Cr_2O_3 NCs via co-precipitation method.

systematically with a co-precipitation route (B2), with both synthesis pathways featuring a critical microwave-assisted crystallization step. Microwave irradiation was essential for developing a unique nanocomposite morphology, providing the necessary rapid, uniform volumetric heating to allow immediate nucleation and controlled growth that facilitated the formation of specialized nanostructures responsible for improved material properties.[10] The morphology obtained by the process is responsible for the improved barrier properties as it provides more tortuous paths for corrosive species.[11]

The originality of this work is therefore threefold: First, it demonstrates the viability of a green synthesis method for producing high-performance anti-corrosion NCs tunable in morphology. Second, characterization (XRD, FESEM, EDS, AFM, FT-IR) of the synthesized (NCs) establishes that composites with notably different chemical compositions (Ni/Cr ratio of ~1.3 for B1 against ~2.3 for B2) may possess comparable corrosion inhibition efficiency (~82%). Third, we reveal a stoichiometry-independent barrier mechanism that operates effectively in corrosion inhibition, supported by recent advances in nanomaterial design principles.[12] The novelty of this work is twofold: first, the development of an environmentally friendly synthesis route that integrates direct calcination of mixed metal-salt pastes with co-precipitation and subsequent microwave irradiation—an unconventional combination not previously reported for producing NiO/Cr_2O_3 nanocomposites; and second, the formation of a distinctive micro-lobed morphology that significantly enhances the physical barrier properties for corrosion protection, independent of stoichiometric variations.

Materials and methods

The forerunner material applied for the production of Cr_2O_3 NPs was chromium acetate (Merck Chemicals); meanwhile, for NiO NPs synthesis, nickel acetate (Merck Chemicals) was used. Multiple techniques were employed for sample characterization: scanning the morphology and image of the sample using an electron microscope (FESEM); compound compositions were examined using energy-dispersive X-ray spectroscopy (EDS) via a TESCAN MIRA3 microscope operating at 20 kV. To inspect the crystal structure of the prepared compounds, an X-ray diffraction (XRD) Bruker D8 Advance diffractometer with Cu Kα radiation ($\lambda = 1.5406$ Å), scanning range of 10–80° (2θ), was used. Bruker Multimode 8 was employed in AFM tapping mode and was used to examine the topography of all the prepared samples. Finally, the spectra from FT-IR of the entire designed samples were verified by a Shimadzu IRTracer-100 spectrometer using KBr pellets (4000–400 cm^{-1} range).

Synthesis of NiO/Cr_2O_3NCs via direct thermal decomposition method

This low-cost/environmentally friendly method was used to synthesize NiO/Cr_2O_3NCs via a simple enhanced route by weighing 1 gm of nickel salt and dissolving it in deionized water until a paste was formed followed by adding 1 ml of (1)M of KOH to the paste, in a different beaker 1 gm of chromium acetate was dissolved in deionized water until a paste was formed followed by adding 1 ml of (1)M of KOH to the paste; then the whole materials were mixed in a crucible and heated for 1 minute at 80 °C. A black

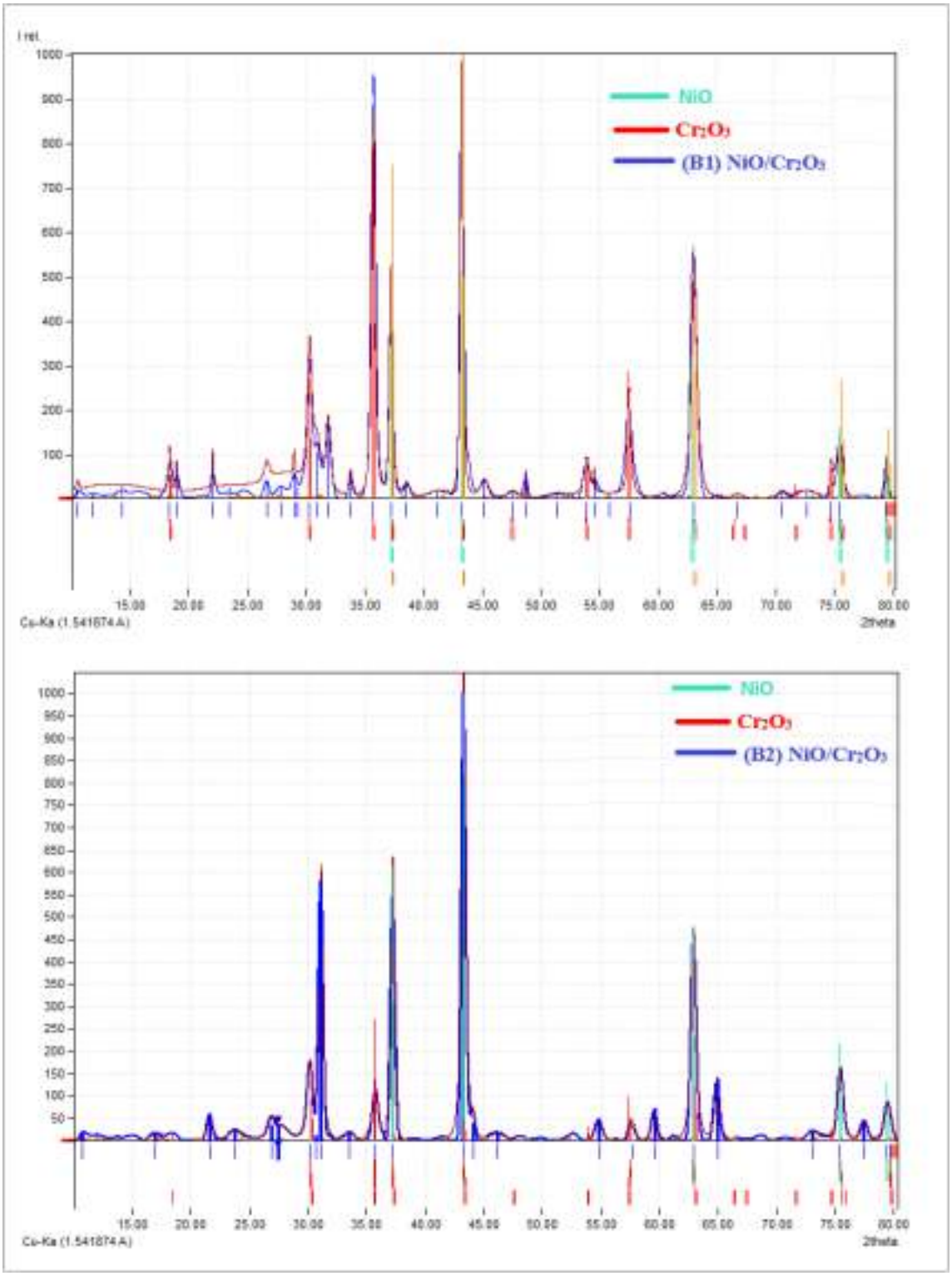

Fig. 1. XRD patterns of NiO/Cr_2O_3 NCs synthesized by direct calcination method (B1) and Co-PPT method (B2) respectively.

precipitate was formed directly; then the crucible was transferred to a closed chamber oven and went through calcination for 2 hours at 850 °C, followed by placing the precipitate in a microwave oven for 2 min at (900 W)[10,11] as in Scheme 1a. The sample was donated as (B1).

Synthesis of NiO/Cr_2O_3 NCs via the co-precipitation method

This method was used to synthesize NiO/Cr_2O_3 NCs via simple, efficient steps by preparing (0.1) M nickel salt and (0.1) M chromium acetate in separate beakers. These salts were mixed in a beaker heated with stirring for 15 minutes at 80 °C. Drops of 10 ml of 1 M KOH were added gradually to the mixture, and a change in the solution color was observed from bluish green to a darker color; the solution was left for 2 hours at 80 °C, then transferred into a crucible and went through calcination for 2 hours at 850 °C. A black precipitate was formed directly; then the crucible was transferred to a microwave oven for 2 min at (900 W)[10,11], as in Scheme 1b. The sample was donated as (B2).

Table 1. The calculated crystallite size for all samples (B1and B2).

Samples	2-Theta	FWHM	Size(nm)
B1	43.080	0.404	22.93
B2	42.960	0.384	23.24

Results and discussion

X-ray diffraction

XRD patterns in Fig. 1 show all the achieved products in which NiO/Cr_2O_3 NCs were synthesized by the direct calcination method (B1) and Co-PPT method (B2) assisted by microwave radiation, respectively. For each sample, the mean particle size was calculated according to the formulation of Debye Scherrer, $D = 0.9\lambda/(\beta\cos\theta)$. Where D is the average crystalline size, while λ is for Cu-Kα ($\lambda = 0.1542$ nm), β points to (FWHM), while (θ) is the Bragg's angle.[13,14] The XRD peaks for all samples (B1, B2) were donated by the occurrence of noticeable peaks at 24.4, 28.4,

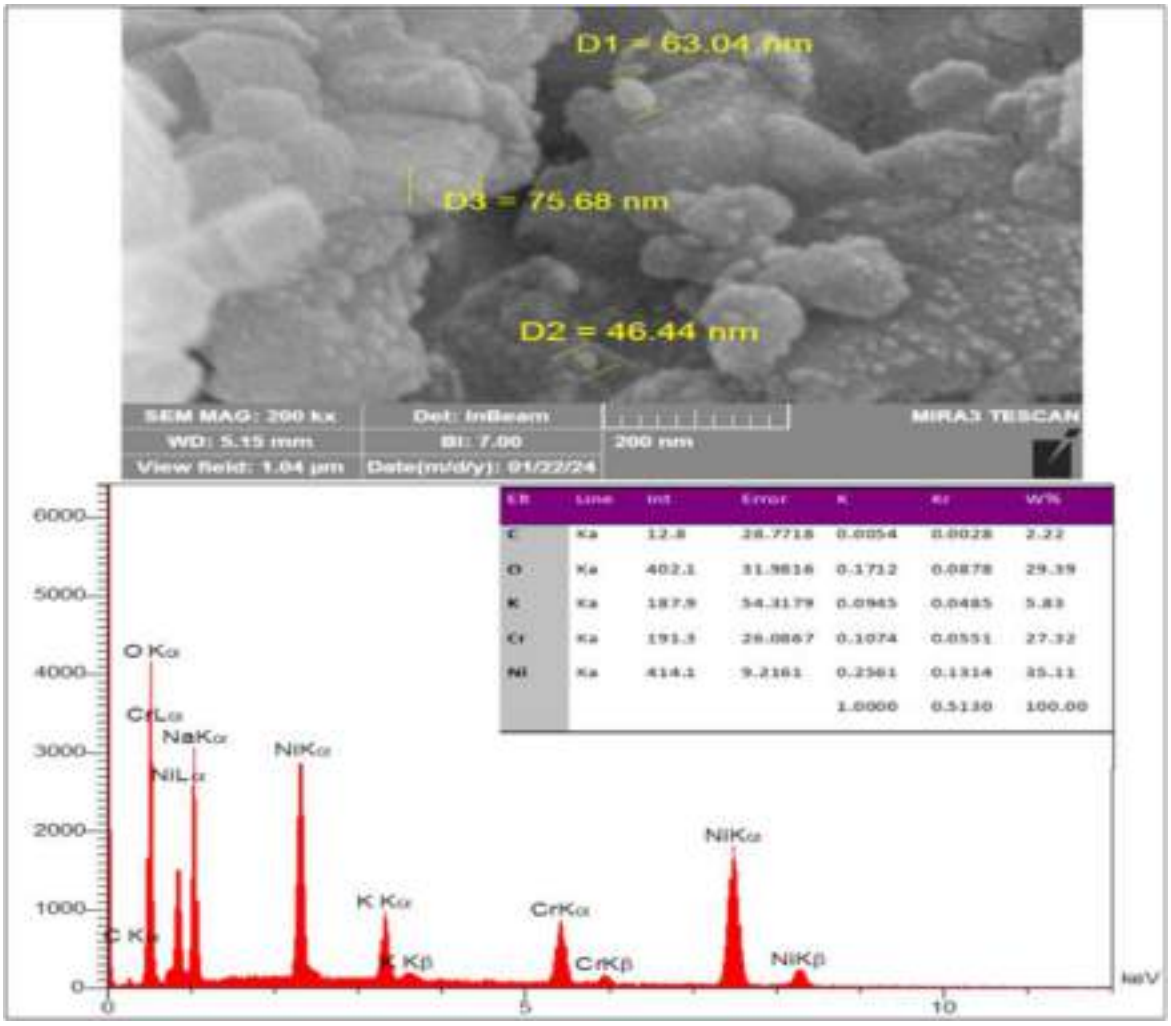

Fig. 2. Surface morphology of (B1) sample; FESEM - EDS images of NiO/Cr_2O_3 NCs synthesized by direct calcination method.

33.5, 36.1, 41.4, 43.1, 50.1, 54.8, 63.2, 65, and 72.9° sideways with following lattice planes (0 1 2), (2 2 0), (1 0 4), (1 1 0), (1 1 3), (4 0 0), (0 2 4), (1 1 6), (2 1 4), (3 0 0) and (119) respectively[6] as in Table 1. The dimensions of the average crystalline were (40) nm. As well, the presence of peaks of high intensity signifies the formation of pure crystals of NiO/Cr_2O_3 NCs. The calculated crystallite size for the (311) plane for both samples (B1–B2) is included in Table 1. The average crystalline size was calculated for (B1–B2) via the Debye-Scherrer formula and was found to be (22.93 and 23.24) nm. Generally, the size and usage of the prepared nano NiO and Cr_2O_3 oxides can differ depending on the specific application and desired properties.[15,16] In all samples, no other impurities could be observed in the XRD pattern; however, the literature explains that if broad peaks were witnessed in the XRD pattern, this indicates that the full

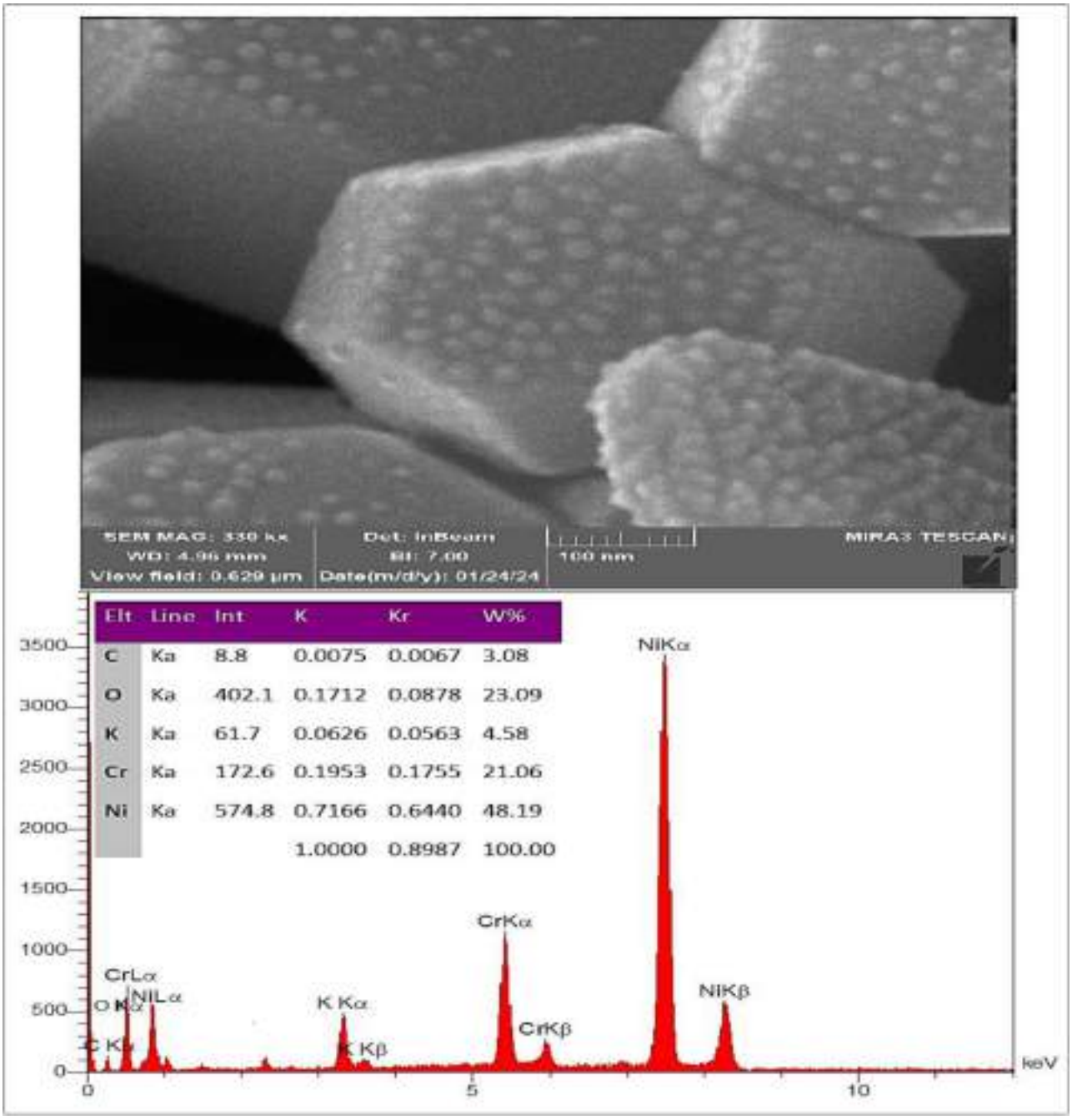

Fig. 3. Surface morphology of (B2) sample; FESEM -EDs image of of NiO/Cr_2O_3 NCs synthesized by Co-PPT method.

width-.half maxim(FWHM) value is high, and therefore the average particle size of the designed sample is smaller. Noticeable peaks in the XRD pattern indicate the well-crystalline nature of the designed sample and that the full width half maximum value is smaller; thus, indicating a larger average crystallite size. [13,16]

Surface morphology via FESEM and EDS techniques

The morphology of the typically synthesized NiO/Cr_2O_3-NCs was investigated by FE.SEM and E.DS, as in Figs. 2 and 3, the obtained results for all samples were in good alignment with previous literature. [8,17] For all the prepared samples, FESEM images showed interesting shapes: aggregated cubical $NiO\text{-}Cr_2O_3$ NCs for both (B1) and the shape of the (B2) sample was found to be dotted quasi-cubic $NiO\text{-}Cr_2O_3$ NCs. Manufacturing the samples via calcination and Co-ppt methods, assisted by microwave discrete radiation, possibly led to obtaining the particular shape for all engineered samples; moreover, it resulted in good crystallinity due to unvarying heating and precise control of processing parameters, which ultimately led to phase purity enhancement. Therefore, sample synthesis with microwave radiation is considered an attractive approach for fabricating crystalline NCs with customized properties for various field applications. [7–9] The FESEM images reveal a micro-lobed, segmented morphology resembling the surface pattern of a bio-inspired hierarchical micro-lobed architecture. This hierarchical structure is believed to enhance the nanocomposite's adhesion to the steel surface and provide a tortuous path for corrosive species, thereby improving barrier performance. The EDS spectrum of sample (B1) showed high intensity peaks of nickel ranging from 35.11 wt%, peaks of chromium ranging from 27.32 wt% and of oxygen ranging from 29.39% of oxygen respectively, which is a further indication of the presence of Ni_XO_y and Cr_xO_y. While the EDS spectrum of sample (B2)

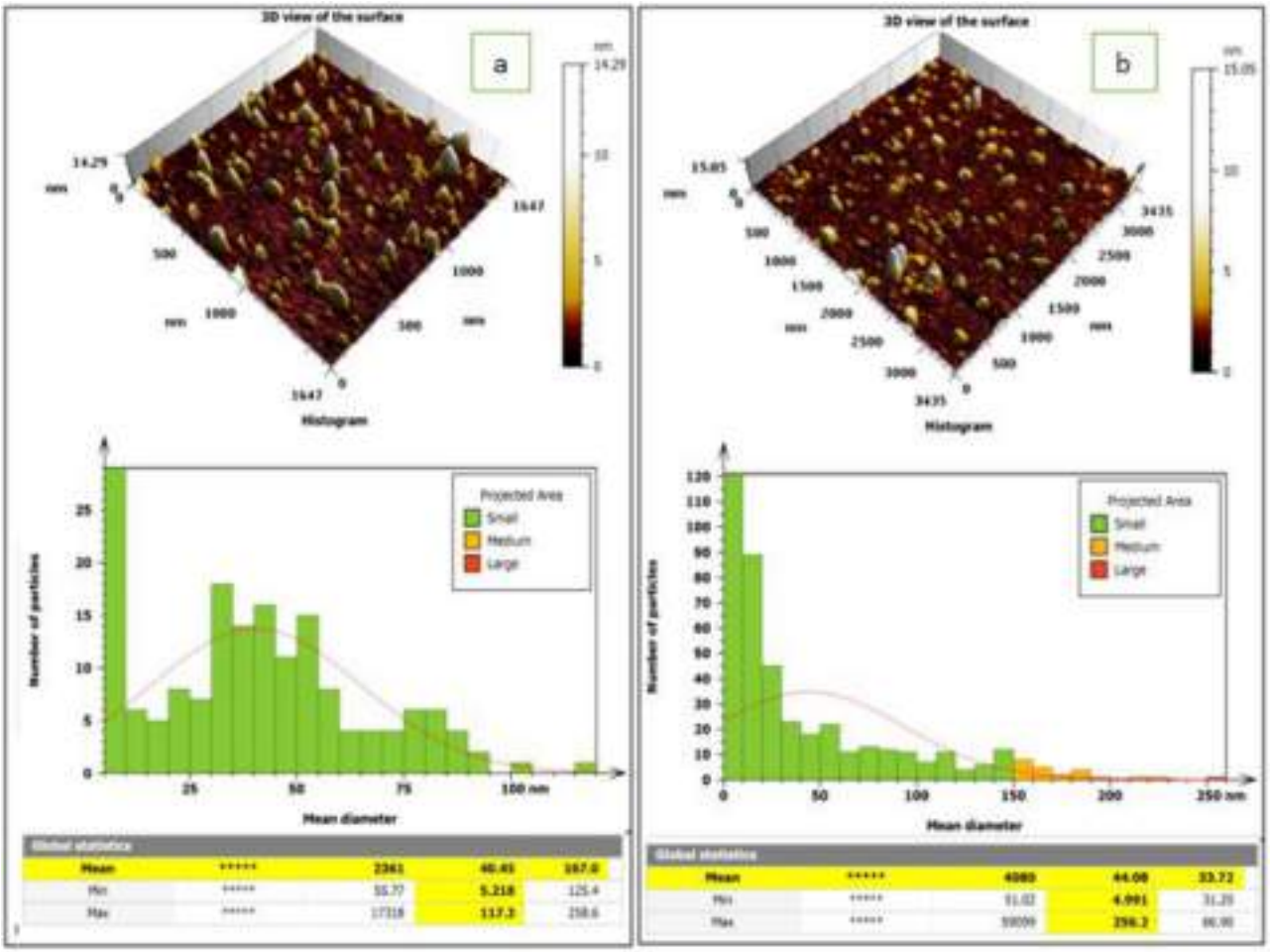

Fig. 4. (a) AFM image of EDs image of NiO/Cr_2O_3 NCs synthesized by direct calcination method. (b) AFM image of EDs image NiO/Cr_2O_3 NCs synthesized by Co-PPT method.

showed high intensity peaks of nickel ranging from 48.19 wt % and peaks of chromium ranging from 21.06 wt% and of oxygen ranging from 23.09 wt%, respectively, which is a further indication of the presence of Ni_XO_y and Cr_xO_y. The pronounced purity of the synthesized nanocomposite was shown by EDX mapping analysis.[8,17] Notably, the EDS analysis confirmed the presence of Ni, Cr, and O in the composites, revealing that the Ni/Cr weight ratio was very different between the two samples (~1.3 for B1 vs. ~2.3 for B2), due to their distinct ways of synthesis. This compositional difference did not interfere with the corrosion inhibition performance. XRD patterns matched the reference phases for NiO (JCPDS 47-1049) and Cr_2O_3 (JCPDS 38-1479), indicating the formation of a nanocomposite consisting of distinct NiO and Cr_2O_3 crystallites. Such a result suggests that the mechanism of anti-corrosion is dominated by the physical barrier effect of the nanocomposite layer, irrespective of the precise stoichiometry within the studied range.

Atomic force microscopy (AFM)

2D and 3D AFM data for all prepared samples (B1–B2), respectively, were obtained; in which NiO/Cr_2O_3 –NCs were integrated *via* calcination assisted by (MW-I) radiation and Co-ppt method assisted by (MW-I) radiation, respectively Fig. 4a, b. For each sample, the mean particle size was found to be (40,45 and 44.08) nm, respectively.

Thus, the selected characterization methods in nano-fields are administered by certain data required to investigate the manufactured nano-composites. The Analysis of crystal assembly and phase configuration XRD is superior; meanwhile, detailed morphological data can be provided via the FESEM method, and elemental analysis particulars are typically attained from the EDS technique. Collective usage of these techniques provides inclusive insights into the arrangement, assembly, and morphology of nanocomposites, supporting their characterization and application enhancement.[18,19] The fact that the average crystallite size estimated from XRD (~23 nm) and the particle size measured by AFM lie in the range 40–45 nm is a common feature of polycrystalline nanomaterials. While XRD measures the size of discrete diffracting domains, AFM provides images of the overall particle morphology, which is generally an agglomerate of several such crystalline domains. Such agglomeration is also routinely observed from FESEM images and does not detract from the nanoscale character of the material.

FT-IR spectra analysis

The vibrational modes of NiO/Cr_2O_3 NCs were shown by FT-IR, as in Table 2. using a pellet of KBr in

Table 2. F.T-IR spectra with main bands in (cm^{-1}) of NiO/Cr_2O_3 based nanostructures.

Symb.	ν Cr^{+2}-O	ν Cr^{+3}-O	ν Ni^{+2}-O	δ O–H	ν $H_2O$of Hydration
B1	669.03	449.35	422.36	1641.65	3450.41
B2	619.11	565.10	443.60	1645.17	3419.56

* δ =bending, *v =stretching.

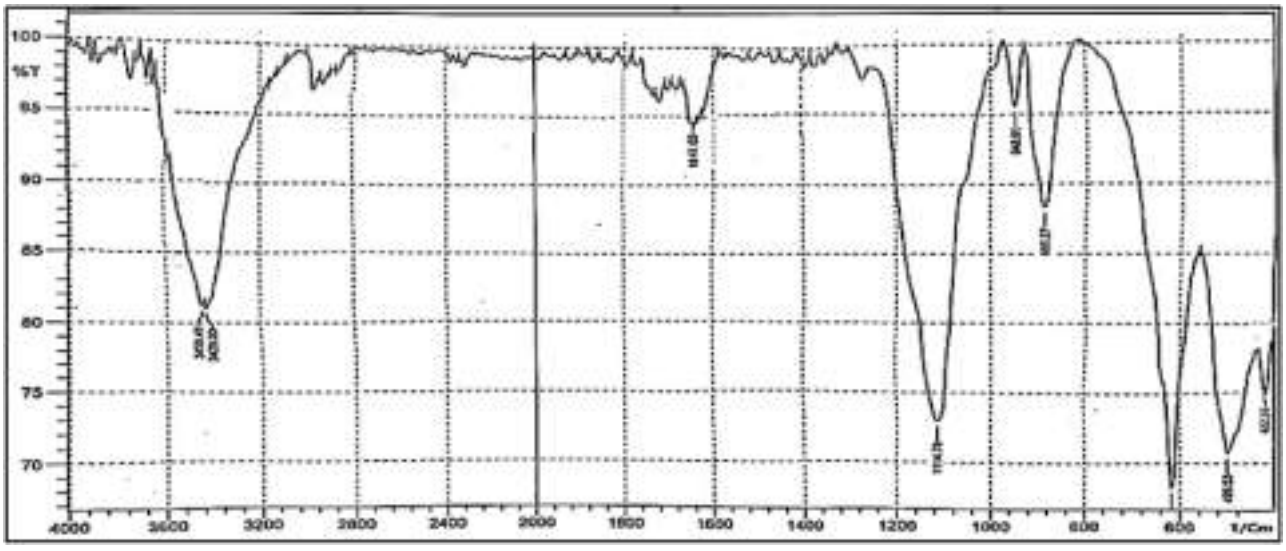

Fig. 5. FT-IR Image of NiO/Cr_2O_3 NCs synthesized by direct calcination method.

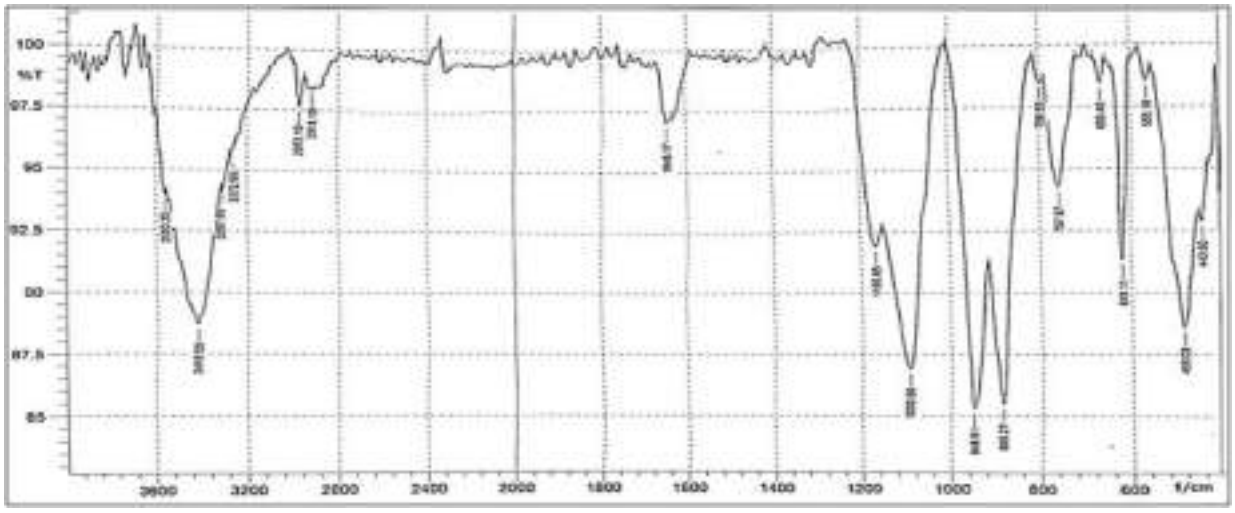

Fig. 6. FT-IR Image of NiO/Cr_2O_3 NCs synthesized by Co-PPT method.

Table 3. Chemical composition of carbon steel C45.

Metal	C%	Si%	Mn%	S%	P%	Cu%	Ni%	Cr%	Fe%
Carbon Steel 45	0.36–0.42	0.15–0.30	1.00–1.40	0.05	0.05	0.50	0.20	0.20	96.88–97.49

the wavelength range 4000–400 cm^{-1}. FT-IR data of NiO/Cr_2O_3 –NCs prepared via calcination method in Fig. 5 exhibited peaks fixed at 3450 and 1641 cm^{-1} fit to the hydration water that has stret. ching-bending vibration of hydroxyl groups (O–H) correspondingly. Peaks at 948 and 422 cm^{-1} are credited to C-O / Ni-O [20,21] stretching vibrations. Additionally, the binary broad band at 669 and 499.53 cm^{-1} credited to Cr^{+2}-O, Cr^{+3}-O vibrations.

FT-IR image of NiO/Cr_2O_3 –NCs primed via Co-ppt method in Fig. 6, shows wide-ranging peaks fixed at 3432 and 1614 cm^{-1} fit to the hydration water that has stret. ching-bending vibration of hydroxyl groups (O–H) correspondingly. Peaks at 948 and 443 cm^{-1} are credited to C-O / Ni-O [20] stretching-vibrations. Additionally, the binary broad band that appears at 619 and 565 cm^{-1} is credited to the vibrations of Cr^{+2}-O, Cr^{+3}-O. [21] These outcomes evidently supported the synthesis of the nanocomposite of the prepared samples. The observed shifts in Cr–O and Ni–O vibrational bands between B1 and B2, as shown in Table 2, are attributed to differences in Ni/Cr stoichiometry and crystalline ordering induced by the two synthesis methods. These variations confirm the successful formation of nanocomposites with distinct local bonding environments, which nevertheless yield similar corrosion inhibition efficiencies.

Corrosion measurements

A Host computer was included in the potentiostat setup, a thermostat, and a magnetic stirrer, alongside the potentiostat and galvanostat. The pyrex-cell capacity is 250 ml, consisting of internal and external plates. Potentiodynamic polarisation measurements were carried out to study the corrosion performance of the synthesized NiO/Cr_2O_3 nanocomposites. A three-electrode electrochemical cell with a carbon steel (C45) working-electrode, and a platinum counter electrode, and a saturated calomel reference electrode (SCE) was used.

Working electrode preparation

The carbon steel electrode surface was ground sequentially with SiC abrasive paper up to 1200 grit, followed by polishing with 0.5 μm alumina slurry to a mirror finish. Afterwards, the electrode was cleaned ultrasonically in acetone for 5 minutes, rinsed with distilled water, and dried. [22] All the experiments were conducted at 298 K, ruled by a cooling-heating-circulating water bath in 0.1 M HCl solution. The open-circuit-potential, Eocp, was monitored for 15 minutes in order to attain a steady state. Polarization curves were acquired by scanning the potential from –200 mV to + 200 mV versus Eocp with a scan rate of 1 mV/s. All measurements were performed in triplicate to ensure reproducibility. [23]

Table 4. Corrosion factors in HCl solutions for blank and compound.

Comp.	–Ecorr (mV)	icorr (μA/cm^2)	I corr./ r (A/cm^2)	Resis. (Ω)	–Bc (mV/Dec)	Ba (mV/Dec)	Corr. rate, (mm/y)	IE%
Blank	–0.385	563.2	0.001	28.96	0.055	0.120	5.529	–
B1	–0.789	99.76	1.995E-4	1352	0.605	0.638	0.979	**82**
B2	–0.825	98.51	1.970E-4	1420	0.692	0.603	0.967	**81**

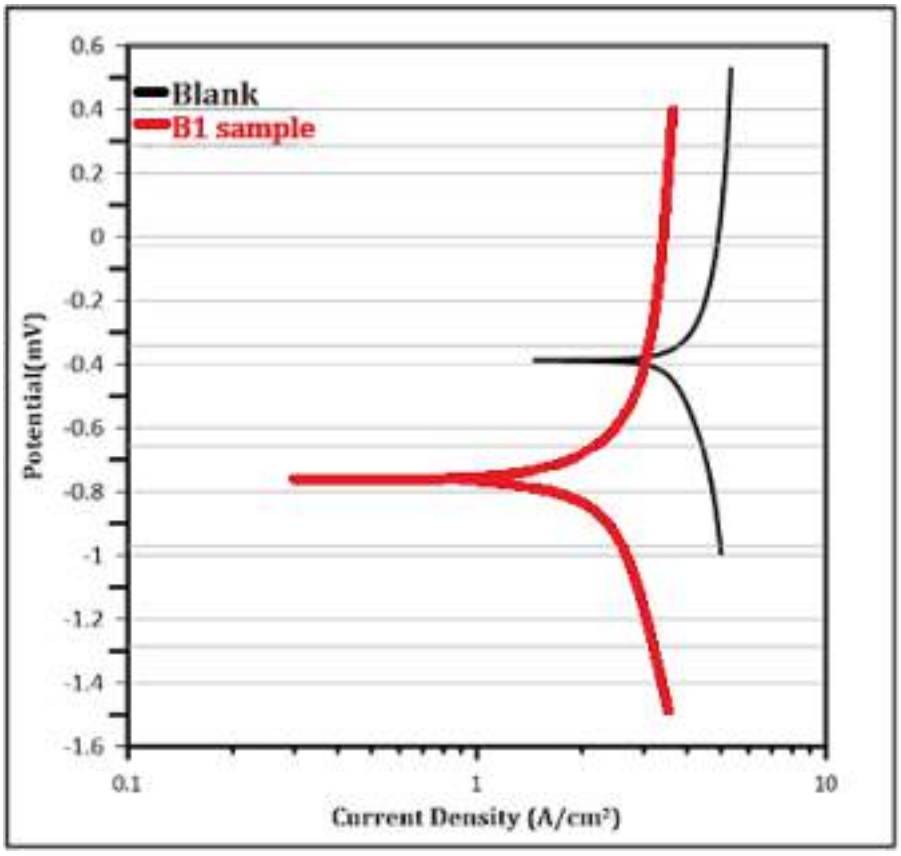

Fig. 7. Polarization curves for corrosion of blank HCl + (B1 sample) solution.

Polarization curves

The evaluation of resulting data obtained from corrosion parameters can be tracked in Tables 3 and 4 The corrosion current density (icorr) and corrosion potential (Ecorr) were obtained by the extrapolation of the cathodic-anodic Tafel with/without inhibitor molecules in HCl (0.1 M) solution. The anodic (ba)-cathodic (bc) Tafel slopes obtained from Figs. 7 and 8. Table 4 shows the resulting data of the corrosion potential Ecorr (mV), corrosion current density icorr (A/cm^2), cathodic-anodic Tafel slopes (mV/Dec), and protection efficiency PE%.[24,25] The large negative shift in the Ecorr value of both samples, B1 (–789 mV) and B2 (–825 mV), as compared to the blank (–385 mV), implies that NiO/Cr_2O_3 nanocomposites act primarily as a cathodic inhibitor. This means that the protective thin film situated on the surface of carbon steel suppresses the cathodic reaction, such as the reduction of oxygen. A key piece of evidence for their inhibition efficiency is an 80% reduction in corrosion current density, icorr, for both composites, as in Eq. (1).

$$\%IE = \frac{(icorr)\,o - (icorr)}{(icorr)\,o} * 100 \quad (1)$$

Where $(i_{corr})_o$= corrosion current density (with no inhibitors), (i_{corr}) = corrosion current density (with inhibitors).[24,25] The tested sample was inserted into a corrosion cell in which the diameter of the exposed surface to the solution was 16.55 cm2. Scheme 2 shows the complete system set up of polarization measurement.

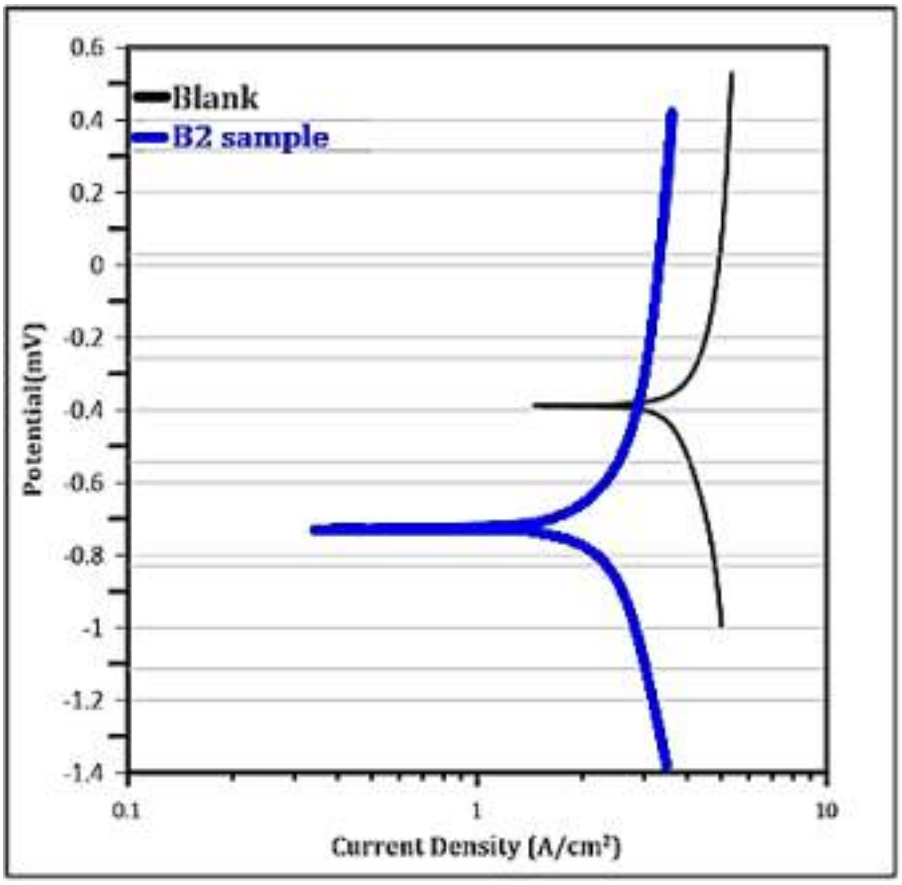

Fig. 8. Polarization curves for corrosion of blank HCl +(B2 sample) solution.

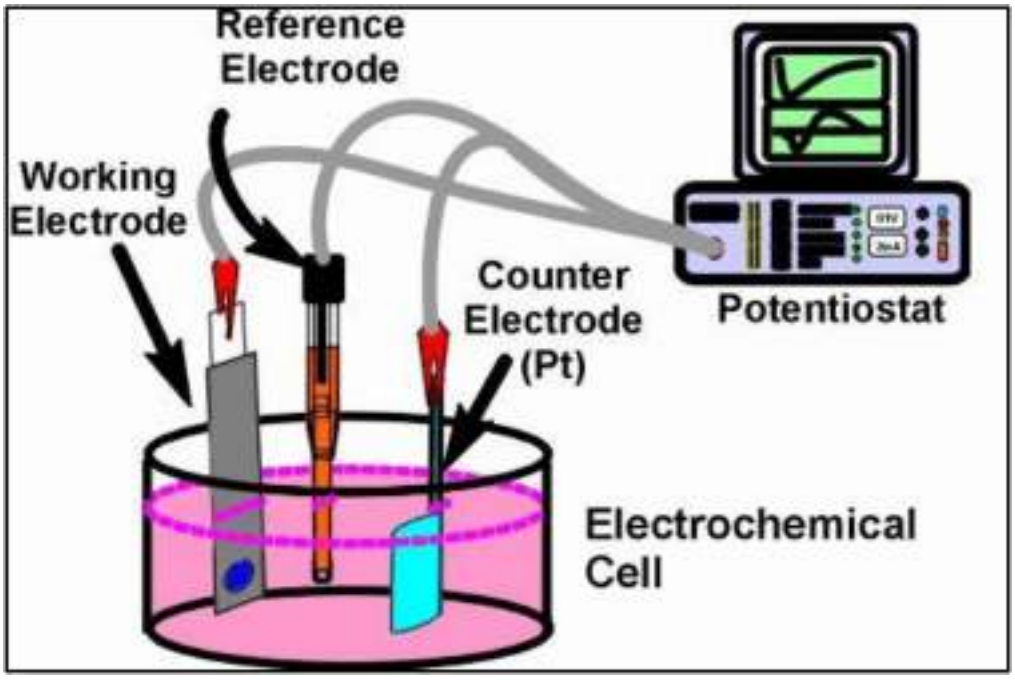

Scheme 2. Corrosion cell set up and its three electrodes.

Conclusion

The current study describes the corrosion performance of NiO/Cr_2O_3 nanocomposites with a unique bio-inspired hierarchical micro-lobed architecture synthesized via direct calcination (green/environmentally friendly method) and co-precipitation methods. Characterization techniques were performed using five complementary techniques: XRD for crystal structure, FESEM/EDS for morphology and composition, AFM for topography, and FT-IR for functional groups. The most important finding in this work is that despite the quite different chemical compositions of both composites, both showed, remarkably, similar corrosion inhibition efficiencies of ~82% in 0.1 M HCl. This particular hierarchical structure enhances adhesion to the steel surface and allows the easy formation of a dense protective barrier layer. Although the corrosion inhibition efficiency remained stable (~82%) across the Ni/Cr ratios studied (~1.3–2.3), it is anticipated that extreme stoichiometric deviations could affect barrier layer integrity. Future studies exploring a wider compositional range are recommended to define the optimal stoichiometric window for corrosion protection. This work illustrates that the anti-corrosion performance is effectively independent of the Ni/Cr ratio variations, underlining the fundamental role of morphological control in barrier protection mechanisms.

Acknowledgment

The project was supported by Baghdad University-Science College - Chemistry Department, Al-Mustansiriyah University, Dr. Yaseen Ismael Imran, Biotechnology Department, Al-Nahrin University and assistant lecturer Inas Ismael Imran–Department of Computer, College of Education for Women, Baghdad University.

Authors' declaration

- Conflicts of Interest: None.
- I hereby confirm that all the Figures and Tables in the manuscript are mine. Furthermore, any Figures and images that are not mine have been included with the necessary permission for re-publication, which is attached to the manuscript.
- No animal studies are present in the manuscript.
- No human studies are present in the manuscript.
- Ethical Clearance: The project was approved by the local ethical committee at Al-Mustansiriyah University.

References

1. Koch G. Cost of corrosion. In Trends in Oil and Gas Corrosion Research and Technologies. Woodhead Publishing, 2017. https://doi.org/10.1016/B978-0-08-101105-8.00001-2.
2. Yousif QA, Abbas AA, Khalaf RM, Ahmed SA. High-performance corrosion inhibitors for carbon steel in hydrochloric acid: electrochemical and DFT studies. RSC Adv. 2025;15:28666–28688. https://doi.org/10.1039/D5RA04952K.
3. Zhang Y, Li X, Wang C, *et al.* Recent advances in metal oxide nanocomposites for corrosion protection. Prog Mater Sci. 2022;124:100868. https://doi.org/10.1016/j.pmatsci.2021.100868.
4. Zhou W, Chen H, Liu Y. Cr_2O_3 based nanocomposites for high-temperature corrosion protection. Corros Sci. 2023;214:111002. https://doi.org/10.1016/j.corsci.2023.111002.
5. Li H, Zhang R, Wang X. Nickel oxide nanostructures: Recent advances in synthesis and corrosion protection applications. Appl Surf Sci. 2023;608:155132. https://doi.org/10.1016/j.apsusc.2022.155132.
6. Wang X, Liu Y, Zhang J. Synergistic effects in mixed metal oxide nanocomposites for enhanced functional performance. ACS Appl Mater Interfaces. 2022;14(15):17812–17824. https://doi.org/10.1021/acsami.1c23456.
7. Al-Hada NM, Alsabah KK, Al-Obaidi HS, Al-Najar LS, Al-Dulaimy TG, Al-Ameri BA. Nanofabrication of (Cr_2O_3)x (NiO)1-x and the impact of precursor concentrations on nanoparticles conduct. J Mater Res Technol. 2021 Jan;11:252–263. https://doi.org/10.1016/j.jmrt.2021.01.007.
8. Maheshwaran G, Ramachandran S, Kumar P, Chandra S, Singh R, Patel V, *et al.* Exploration of Cr_2O_3.NiO nanocomposite as a superior electrode material for supercapacitor applications. Mater Lett. 2021 Jun;300:130191. https://doi.org/10.1016/j.matlet.2021.130191.
9. Chen L, Wang H, Zhang K. Recent advances in Cr2O3based nanocomposites for photocatalytic applications. J Environ Chem Eng. 2023;11(2):109487. https://doi.org/10.1016/j.jece.2023.109487.
10. Liang S, Zhu L, Gai G, Yao Y, Huang J, Ji X, Zhou X, Zhang D, Zhang P. Synthesis of morphology-controlled ZnO microstructures via a microwave-assisted hydrothermal method and their gas-sensing property. Ultrason. Sonochem. 2014;21(4):1335–1342 https://doi.org/10.1016/j.ultsonch.2014.02.007.
11. Wang L, Zhao F, Liu T, Chen P, Huang Y, Xu R. Bio-inspired micropatterned epoxy coating for enhanced barrier and anti-corrosion performance. Corros Sci. 2024;228:111818. https://doi.org/10.1016/j.corsci.2024.111818.
12. Yang J, Smith A, Johnson B. New paradigms in nanomaterial design for corrosion protection: Beyond traditional composition-based approaches. Nat Commun. 2024;15(1):1234. https://doi.org/10.1038/s41467-024-45679-0.
13. Guillén C, Herrero J. Structural changes induced by heating in sputtered NiO and Cr_2O_3 thin films as p-type transparent conductive electrodes. Electron Mater. 2021 Mar;2(2):49–59. https://doi.org/10.3390/electronicmat2020005.
14. Gao X, Li J, Zhao Y, Wang H, Chen L, Sun Z, *et al.* Synergizing aliovalent doping and interface in heterostructured NiV nitride@oxyhydroxide core-shell nanosheet arrays enables efficient oxygen evolution. Nano Energy. 2021 Jul;85:105961. https://doi.org/10.1016/j.nanoen.2021.105961.

15. Mohammad EJ, Kareem MM, Abbas AM. Preparation of MWCNTS/Cr_2O_3-NiO nanocomposite for adsorption and photocatalytic removal of Bismarck brown G dye from aqueous solution. Indones J Chem. 2020 May;20(3):554. https://doi.org/10.22146/ijc.43429.
16. Sharma UR, Sharma N. Green synthesis, anti-cancer and corrosion inhibition activity of Cr_2O_3 nanoparticles. Biointerface Res Appl Chem. 2020 Jul;11(1):8402–8412. https://doi.org/10.33263/BRIAC111.84028412.
17. Khalid A, Mahmood A, Numan A, Khalid M, Iqbal M, Mansoor MA. Facile synthesis and electrochemical study of NiO–Cr_2O_3/carbon nanotubes/polyaniline hybrid as a high-performance supercapattery electrode material. J Alloys Compd. 2025;1031:181009. https://doi.org/10.1016/j.jallcom.2025.181009.
18. David SA, Doss A, Pole RPP. Biosynthesis of chromium oxide nanoparticles by Momordica charantia leaf extract: Characterization and their antibacterial activities. Results Surfaces Interfaces. 2023 May;11:100120. https://doi.org/10.1016/j.rsurfi.2023.100120.
19. Ferenji AE, Hassen YE, Mekuria SL, Kebede FA, Tadesse AG, Getachew B, *et al.* Biogenic mediated green synthesis of NiO nanoparticles for adsorptive removal of lead from aqueous solution. Heliyon. 2024 May;10(11):e31669. https://doi.org/10.1016/j.heliyon.2024.e31669.
20. Al-Kalifawi EJ, Al-Obodi EE, Al-Saadi TM, Al-Hamdi RA, Al-Hashimi BA, Al-Yazidi KA, *et al.* Characterization of Cr_2O_3 nanoparticles prepared by using different plant extracts. Acad Publish. 2020 Mar 20;8(3):52–58. https://doi.org/10.15413/ajb.2020.0104.
21. Alhato AY, Kumar R, Barakat MA. Integrated ozonation Ni-NiO/Carbon/g-C3N4 nanocomposite-mediated catalytic decomposition of organic contaminants in wastewater under visible light. Nanomaterials. 2024 Jan;14(2):190. https://doi.org/10.3390/nano14020190.
22. Zhang Y, Liu B, Wang L, Zhang J, Li Q. Design and application of novel nanocomposite coatings for enhanced corrosion protection of carbon steel: Detailed methodology on surface pretreatment. Mater Des. 2025;237:112521. https://doi.org/10.1016/j.matdes.2025.112521.
23. Chen X, Wang H, Liu F, Sun K, Wu S, Zhou Y. Statistical significance and reproducibility in electrochemical corrosion testing: A guide to proper data reporting and replication. ACS Appl Mater Interfaces. 2024;16(10):12769–81. https://doi.org/10.1021/acsami.3c18547.
24. Alqudsi AM, Saleh KA. Conducting polyanethole/metals oxides nanocomposites for corrosion protection and bioactivity. Baghdad Sci J. 2024 Apr;21(4):Article 19. https://doi.org/10.21123/bsj.2023.8458.
25. Ali MDM, Husseini M, Khudhair NA. Impact of wastewater on ditches of rainwater drain in Al-Hilla city. IOP Conf Ser Earth Environ Sci. 2021 Nov;877(1):012007. https://doi.org/10.1088/1755-1315/877/1/012007.

الهندسة المبتكرة في تحضير متراكبات نانوية من أكاسيد النيكل وأكاسيد الكروم واستخدامها في دراسات مقاومة التآكل

سحر أسماعيل عمران

قسم العلوم الاساسية، كلية طب الاسنان، الجامعة المستنصرية، بغداد، العراق.

الخلاصة

تم تصنيع مركبات نانوية من أكسيد النيكل/أكسيد الكروم (NiO/Cr_2O_3) باستخدام طريقتين مختلفتين: الأولى: عملية التكليس المباشر (العينة B1) لأملاح النيكل والكروم في بوتقة داخل حجرة فرن مغلقة، متبوعا باستخدام اشعة الميكروويف؛ مما يوفر نهجًا صديقًا للبيئة خالٍ من نفايات الغازات والسوائل. الثانية: تقنية الترسيب المشترك التقليدية باستخدام اشعة الميكروويف (العينة B2). أنتجت كلتا الطريقتين مورفولوجيا جديدة ومبتكرة ذات فصوص دقيقة تشبه نمط الخنفساء. دُرست تأثيرات مقاومة التآكل لكلتا العينتين. تم توصيف (NiO/Cr_2O_3 NCs)باستخدام تقنيات حيود الأشعة السينية (XRD)، والمجهر الإلكتروني لمسح الانبعاثات (FESEM)، ومطياف الأشعة السينية المشتتة من الطاقة (EDS)، ومجهر القوة الذرية (AFM)، ومطياف الأشعة تحت الحمراء FT-IR. أكد حيود الأشعة السينية (XRD) متوسط أحجام البلورات 22.93 نانومتر (B1) و23.24 نانومتر (B2)، بينما كشف المجهر الذري (AFM) عن متوسط أحجام الجسيمات 40-45 نانومتر مما يشير إلى بلورات نانوية محددة جيدًا مع الحد الأدنى من التكتل. على الرغم من الاختلاف الكبير في تركيب Ni/Cr في ((B1: ~1.3 مقابل (B2: ~2.3) حسب نتائج EDS، فقد وجد أن كلا (NiO/Cr_2O_3 NCs) يتمتعان بكفاءة تثبيط تآكل مماثلة تبلغ ~82٪ للفولاذ الكربوني في 0.1 مولاري من حمض الهيدروكلوريك، حددت نتائج التحليل الكهروكيميائي الآلية الأساسية لعمل المركبات النانوية الناتجة كموانع فعالة ضد التأكل, حيث أنها تعمل على تكوين طبقة واقية على سطح الفولاذ. توضح هذه النتائج أن أداء مقاومة التآكل يحكمه إلى حد كبير تكوين الحاجز واقي ضد التأكل ، مما يثبت صحة كلا طريقتي التصنيع كاستراتيجيات مستدامة لتصميم مركبات النانوية عالية الأداء من NiO/Cr_2O_3 كمواد مضادة ومانعة للتآكل بشكل فعال.

الكلمات المفتاحية: طريقة الترسيب المشترك ، مقاومة التأكل، طريقة الكلسنة المباشرة، أكاسيد المعادن النانوبة ، الخصائص المورفولوجية، الخصائص الهيكلية.